NJC

New Journal of Chemistry

A journal for new directions in chemistry

Accepted Manuscript

This article can be cited before page numbers have been issued, to do this please use: M. Cacicedo, M. C. Ruiz, S. Scioli Montoto, M. E. Ruiz, M. Fernandez, R. M. Torres Sanchez, E. J. Baran, G. R. Castro and I. Leon, *New J. Chem.*, 2019, DOI: 10.1039/C9NJ01634A.

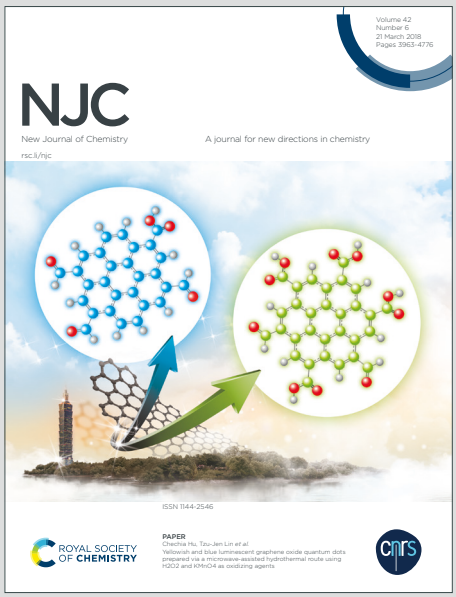

DOI: 10.1039/C9NJ01634A

Lipid nanoparticles – Metvan: reveling a novel way to deliver a vanadium compound to bone cancer cells

Cacicedo M.L.[1], Ruiz M.C.[2], Scioli-Montoto S.[3], Ruiz M.E.[3], Fernández M.A.[4], Torres-Sanchez R.M.[4], Baran E.J.[2], Castro G.R.[1], Leon I.E. *[2]

[1] *Laboratorio de Nanobiomateriales, CINDEFI, Departamento de Química, Facultad de Ciencias Exactas, Universidad Nacional de La Plata (UNLP) -CONICET , Calle 47 y 115, (B1900AJI), La Plata, Buenos Aires, Argentina*

[2] *Centro de Química Inorgánica (CEQUINOR-CONICET- UNLP), Facultad de Ciencias Exactas, Universidad Nacional de La Plata, Bv 120 1465, 1900, La Plata, Argentina.*

[3] *Laboratorio de Investigación y Desarrollo de Bioactivos (LIDeB), Facultad de Ciencias Exactas, Universidad Nacional de La Plata (UNLP), Calle 47 y 115 (B1900AJI), La Plata, Buenos Aires, Argentina.*

[4] *CETMIC (Centro de Tecnología en Minerales y Cerámica) CONICET-CCT La Plata-CICBA, Argentina*

Corresponding author * ileon@biol.unlp.edu.ar

Abstract

Cancer is one of the main causes of mortality worldwide. Common therapy schemes are always based on chemotherapy, radiotherapy and/or surgery. Among chemotherapeutics, vanadium compounds have recently emerged as non-platinum antitumor agents.

In this sense, Metvan ($[V^{IV}O(Me_2phen)_2(SO_4)]$) was identified as one of the most promising vanadium anticancer complexes. In this work, Metvan compound was encapsulated into well designed and developed nanostructured lipid carriers (NLCs) with the aim of improving its biopharmaceutical profile by means of bioavailability, degradation, solubility and cell up-take. A quality by design approach was performed to find the optimal nanoparticle formulation for Metvan delivery. Results exhibited that the ideal formulation was obtained by using myristyl myristate as the lipid matrix and Pluronic F128 as the stabilizing agent with a mean nanoparticle size of 230.8 ± 3.1 nm and a mean surface charge of -7.9 ± 0.8 mV. The formulation showed an encapsulation efficiency of approximately 80% with a drug sustained release for more than 60 h. The kinetic release mechanism of Metvan from nanoparticles fitted Korsmeyer–Peppas model, indicating the Fickian diffusion of Metvan from the nanoparticles. On the other hand, the results showed that the nanoparticles-Metvan system is more effective to decrease cell viability on human osteosarcoma cells (MG-63) than free drug, suggesting a possible

different cell internalization mechanism and intracellular effect.

Introduction

Metal-based compounds are a class of anticancer drugs largely used in the treatment of many kind of tumors, such as lung, prostate, colon, and breast cancers [1–3]. In this sense, vanadium compounds have recently emerged as non-platinum antitumor agents showing promising anticancer activity on several types of solid tumors, mainly on osteosarcoma [4–7].

Regarding these type of substances, 4,7-dimethyl-1,10-phenathroline sulfatooxidovanadium (IV), now known as Metvan, has been identified as a very promising multitarget anticancer vanadium complex effective in different types of cancer cells. Interestingly, Metvan shows high activity against cisplatin-resistant cancer cell lines [8,9]. Also, Metvan at nanomolar and low micromolar concentrations induces apoptosis in several human cancer cell lines such as leukemia, multiple myeloma and solid tumor cells derived from glioblastoma, breast cancer, ovarian, prostate and testicular cancer patients [9,10]. However, despite this promising anticancer activity, no clinical trials were done so far, possibly due to lack of information regarding its speciation in aqueous solution and its thermodynamic/redox stability. Recently, Sanna *et al* reported a complete speciation study of Metvan in aqueous solution and in human blood, as well [11]. The authors suggested that Metvan speciation in blood depends principally on vanadium serum concentration. In this sense, when vanadium concentration was larger than 50 μM, VO^{2+} persisted bound to Me_2phen whilst if vanadium concentration was lower than 10 μM, the VO^{2+} was taken up by the cells. As a conclusion, it was mentioned that the pharmacological activity of Metvan could be a consequence of a synergetic behavior between free Me_2phen, and $V^{IV}O$ and $V^{V}O/V^{V}O2$ species [11]. Le *et al* and Levina *et al* also studied the stability of Metvan in aqueous solutions although with a different perspective. The authors suggested that Metvan undergoes into rapid oxidation to the corresponding V(V) species releasing free ligands within minutes. Results showed that Me_2Phen complexes associated cytotoxicity was equal to the effects of free ligands. The authors arrived to the conclusion that V(IV) complexes played no significant role in the observed biological activities[12,13].

In this sense, it was envisioned to generate a nanocarrier system that encapsulate Metvan complexes to avoid dissociation or interaction with blood components until their entrance

to the target cell. This approach suggested the possibility of optimizing the *in vitro* cytotoxic effect of Metvan against cancer cells.

Encapsulation of active ingredients (AI), metallodrugs included, has been described as a methodology to overcome the biological and biophysical disadvantages that the human body enacts against chemotherapeutic molecules[14]. As part of a project related to the investigation of vanadium complexes with potential anticancer activity, this study deals with the encapsulation of Metvan into well designed and developed nanostructured lipid carriers (NLCs) with the aim of improving its biopharmaceutical profile by means of bioavailability, degradation, solubility and cell up-take. Quality by design (QbD) methodology was used as a tool to optimize NLCs formulation. In this sense, a fractional factorial design was used to simultaneously study the effect of multiple factors over the selected responses or dependent variables: mean particle size, polydispersity index and zeta potential. In addition, a spherical central composite rotatable design (CCD) and the associated response surface (RS) were used for the evaluation and optimization of the design space. Release kinetics, encapsulation efficiency, cell uptake, cytotoxicity and apoptosis studies were performed to determine the behavior of Metvan loaded nanoparticles and their implications against an osteosarcoma human cancer cell line.

Results and discussion

According to the special quality requirements that a nanoparticle formulation needs to reach to be considered efficient and safe for drug delivery applications, some critical quality characteristics were selected and studied [15]. Particle size, surface charge and polydispersity index (PDI) were selected as the responses to be optimized, as they are able to modify the required biopharmaceutical properties.

Screening of pharmaceutical acceptable components was performed to obtain the most appropriate solid lipid/surfactant combination to continue with the optimization process. Four different lipids and surfactants were combined in order to screen the components for NLC preparation. Details about the assayed components are given in the Experimental section. Results showed that all combinations generated did not affect the particles surface charge as the Z-potential remained almost constant at a mean value of -20 mV. On the other hand, particle size and PDI results showed that the best lipid/surfactant combination was Myristyl Myristate (MM) and Pluronic® F127, corresponding to nanoparticle apparent diameter of 159.1 ± 1.0 nm and a PDI of 0.146 (**Table S1**). Pluronic® F127 corresponds to the poloxamers (non-proprietary name) family. These block copolymers

View Article Online
DOI: 10.1039/C9NJ01634A

consist of hydrophilic poly(ethylene oxide) (PEO) and hydrophobic Poly (propylene oxide) (PPO) blocks arranged in A-B-A tri-block structure: PEO-PPO-PEO [16] . The amphiphilic structure of these copolymers allows reaching surfactant properties like the ability to interact with hydrophobic surfaces and biological membranes. Moreover, Pluronic block copolymers have shown the ability to act as potent biological response modifiers capable of sensitizing multidrug resistant (MDR) cancer cells (Kabanov et al., 2002). Finally, MM and Pluronic® F127 were selected as principal compounds to continue with the optimization.

For the fractional factorial design, 16 randomized synthesis were made, and results are shown in **Table 1**.

Table 1: Randomized fractional factorial design with runs and responses in their original coding. Responses: mean particle size (d, nm), polydispersity index (PDI) and zeta potential (Z pot, mV). Fixed effects: amount of lipid (X_1, mg), surfactant percentage in aqueous medium (X_2, w/v%), amount of oil (liquid lipid Crodamol™ GTCC-LQ) (X_3, µl), sonication time (X_4, min) and sonication amplitude (X_5, %).

Run	X_1	X_2	X_3	X_4	X_5	d	PDI	Z pot
1	400	4	10	40	60	208.6	0.200	-7.08
2	100	1	200	10	80	198.5	0.189	-11.37
3	100	4	10	40	80	188.5	0.212	-1.15
4	400	4	200	40	80	191.4	0.208	-1.49
5	400	4	200	10	80	210.7	0.174	-4.49
6	400	4	10	10	60	215.7	0.207	-11.15
7	100	1	200	40	80	201.2	0.118	-5.72
8	100	1	10	10	60	150.2	0.236	-9.56
9	100	1	10	40	60	144.0	0.233	-8.53
10	400	1	200	40	60	245.8	0.158	-16.8
11	400	1	10	40	80	242.6	0.114	-14.48
12	100	4	200	40	60	174.2	0.165	-4.86

View Article Online
DOI: 10.1039/C9NJ01634A

13	100	4	200	10	60	199.5	0.148	-5.45
14	100	4	10	10	80	189.1	0.234	-4.42
15	400	1	10	10	80	240.1	0.184	-14.13
16	400	1	200	10	60	216.2	0.064	-18.14

As it can be seen, mean particle size, PDI and z-potential ranged from 144.0 nm to 245.8 nm, from 0.064 to 0.236 and from -18.14 mV to -1.15 mV, respectively. Statistical analysis indicated that the amount of lipid, the surfactant percentage in aqueous medium and the sonication amplitude were the factors that mainly affect the responses of interest ($p < 0.05$). Therefore, X_1, X_2 and X_5 were further evaluated applying a CCD and a RS methodology (**Table S2**). The other factors (amount of oil and sonication time), were set at 100 µl and 20 minutes, respectively. The adjusted second-order model obtained was as follows:

$$Y = B_0 + B_1X_1 + B_2X_2 + B_3X_5 + B_4X_1X_2 + B_5X_1X_5 + B_6X_2X_5 + B_7X_1^2 + B_8X_2^2 + B_9X_5^2$$

Where B_0 is the intercept and B_1-B_9 are the model coefficients. **Figure 1** shows the contour plots and response surface graphs obtained.

View Article Online
DOI: 10.1039/C9NJ01634A

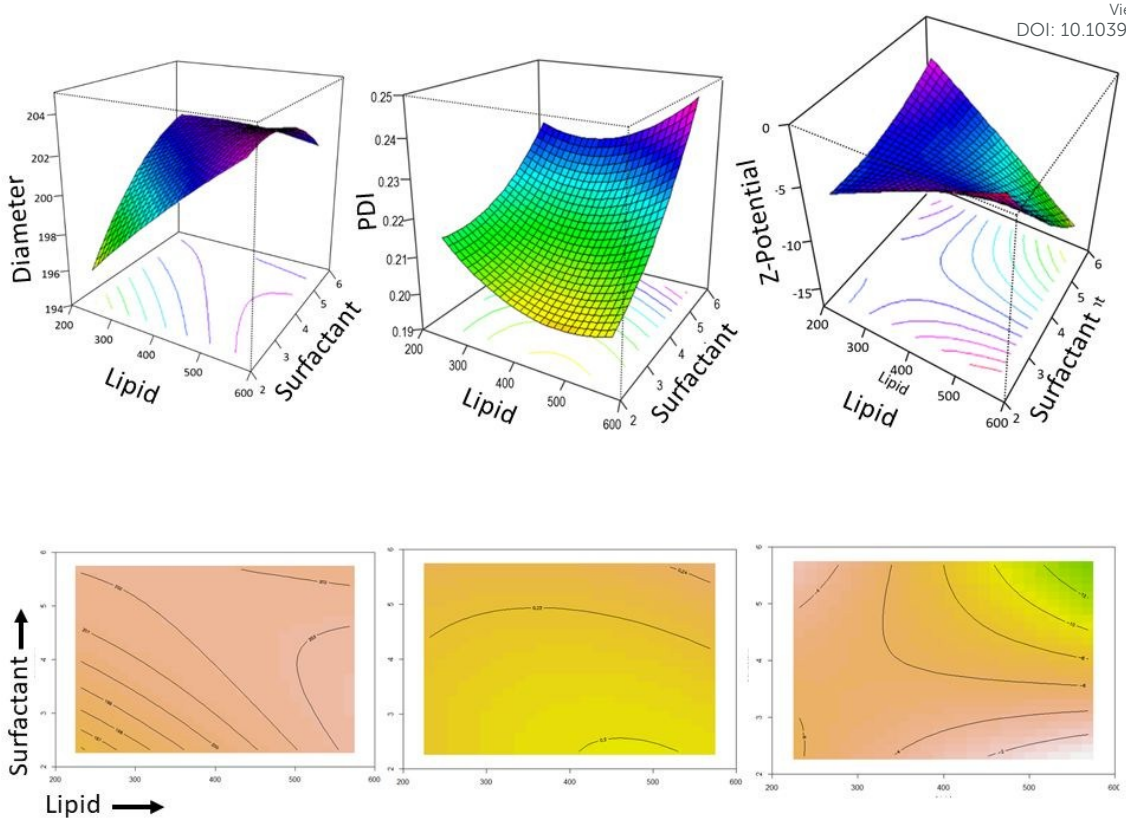

Figure 1. Surface response plots obtained after the nanoformulation design describe the relationship between NLCs parameters (d, PDI and Z-Pot) and synthesis parameters like surfactant and lipid amounts. Contour plots obtained after the nanoformulation design describing relation with NLCs size , PDI and Z-Pot.

Final optimization of the formulation was made using the desirability function approach, which translates and combines the desirability functions for each response into a single function[17]. The desirability value, which defines the closeness of a response to its ideal value, lies between 0 (less desirable) and 1 (most desirable). The point of the highest desirability was found to be at 505.0 mg of lipid, 4.0% p/v of surfactant in aqueous medium and 83% of sonication amplitude. Finally, the optimized formulation was prepared in triplicate to evaluate the accuracy of the anticipated responses, showing predicted errors of 9.06%, 13.30% and 11.97% for particle size, polydispersity index and zeta potential, respectively.

Metvan encapsulation and release from NLCs

Optimized NLC formulation was tested for the encapsulation of Metvan. Basically,

View Article Online
DOI: 10.1039/C9NJ01634A

before the synthesis process, the drug was dissolved in DMSO and then added to the melted lipid. Influence of Metvan in the NLCs structure and morphology measurements on size, PDI and z-potential were performed and compared with the previous results (**Table 2**).

Table 2. NLCs parameters evaluated with and without Metvan payload.

	Size (nm)	PDI	Z pot (mV)
no Metvan	179.16 ± 4,67	0.191 ± 0.006	-16.06 ± 5.08
with Metvan	230.80 ± 5,74	0.235 ± 0.010	-7.29 ± 1.2

AI incorporation into NLCs showed slightly affect two of the three parameters. Nanoparticle apparent diameter was increased to 230.80 ± 5,74 nm, an increment of 28.8%. Moreover, PDI value did not showed significant differences between the formulations. In contrast, particle surface charged turned more near to neutral values increasing from -16.06 ± 5.08 mV to -7.29 ± 1.2 mV. These changes on nanoparticles characteristics were considered acceptable. Additionally, NLCs size and distribution were compared by TEM observations (**Figure 2**).

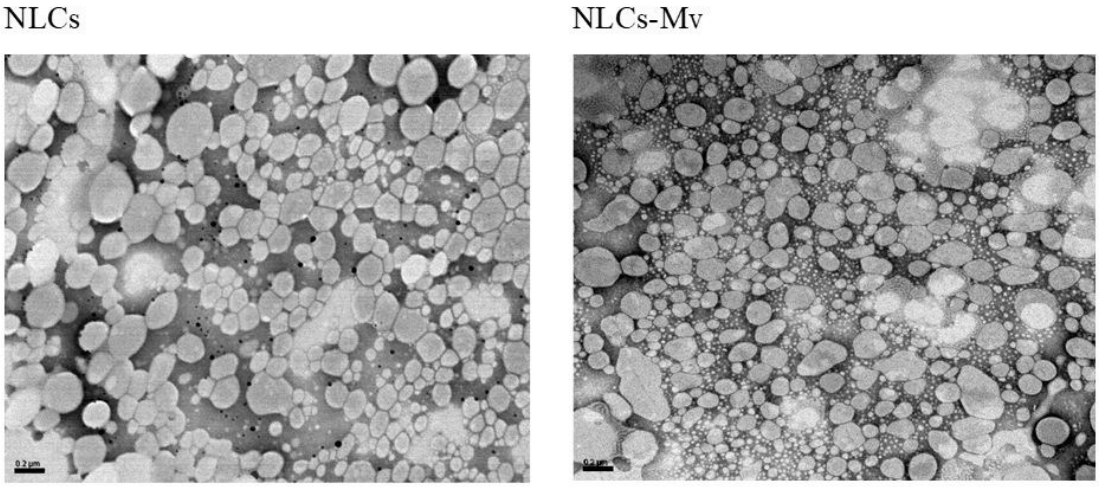

Figure 2. TEM images of nanostructured lipid carriers containing or not Metvan (NLCs-Mv or NLCs respectively).

TEM images exhibited no apparent differences between the formulation with and without drug payload. In both cases, NLCs showed an approximated diameter of 200 nm and a

View Article Online
DOI: 10.1039/C9NJ01634A

well homogeneous population of particles (**Figure 2**). Next, encapsulation efficiency (EE%) and loading capacity (LC%) were evaluated resulting in 77.6 ± 4.8 and 0.022 ± 0.005, respectively. These values enlighten the ability of the developed NLCs to encapsulate the metallodrug with high efficiency.

Metvan release studies were performed in two different conditions of pH. First, Metvan loaded NLCs (NLCs-Mv) were tested under physiologic pH and then at slightly acidic pH of 5.0 (environmental simulation of endocytic structures) [18]. **Figure 3** shows the hyperbolic curves for Metvan released from NLCs after 48 h of incubation at 37ºC. The dependence of drug release with pH showed a preference of the drug to diffuse out of the nanoparticles at pH 5.0, in correlation to what it is expected for these kind of delivery systems. Moreover, both curves exhibited a very similar behavior on the release profile. Initially, Metvan was rapidly released (burst release), followed by a decrease on drug releasing rate. After 48 h the formulations reached Metvan release values of 52.1% and 75.4% for pH 7.4 and 5.0, respectively. Significant differences were found between the amount of released drug at both pHs ($p < 0.05$). The burst release at the beginning might be a consequence of the drug molecules located on the surface of the nanoparticles. In contrast, it could be hypothesized that the drug released in a prolonged way was indeed homogeneously distributed into the nanoparticles lipid core not being able to easily diffuse from them [19]. In order to understand the mechanisms involved in the release process, experimental data was fitted with standard release equations (Eq. 3-5, Experimental Section). Zero order model was avoided because data followed a non-linear pattern, exposing that the diffusion mechanism followed different type of kinetics [20].

View Article Online
DOI: 10.1039/C9NJ01634A

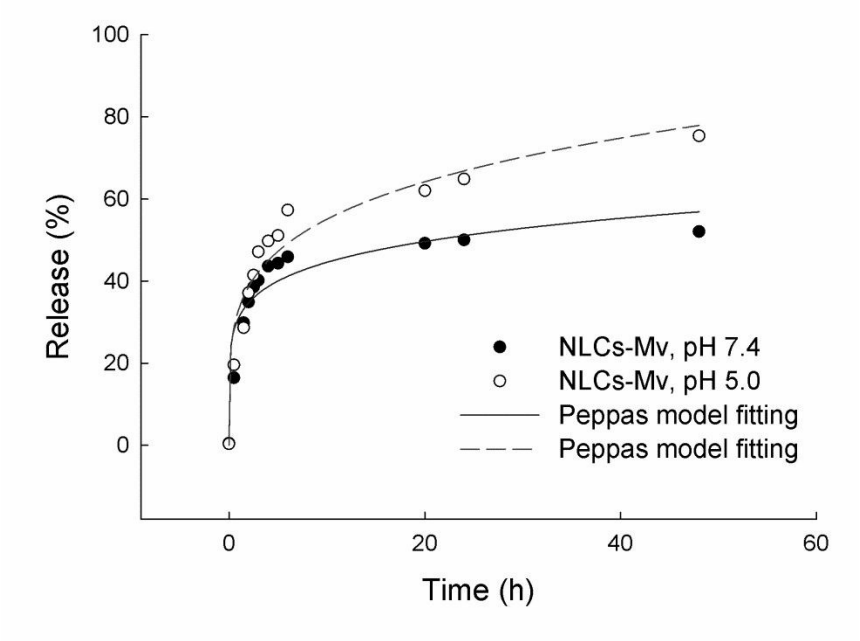

Figure 3. Korsmeyer-Peppas modelling of Metvan kinetic release from NLCs at pH 7.4 and 5.0.

Next, according to the obtained linear correlation coefficient values (R^2) Metvan release fitted a Korsmeyer-Peppas model at both assayed pHs (**Table 3**).

Table 3. Linear correlation coefficient (R^2) for the release kinetics of NLCs-Mv.

	R^2		
NLCs-Mv	First order	Higuchi	Korsmeyer-Peppas
pH 5.0	0.316	0.33	0.94
pH 7.4	0.00	0.00	0.90

This model is based on Fick´s laws and is used to described the release of a drug when more than one mechanism is involved, for example the diffusion of the drug and the degradation of carrier´s structure [21,22]. Moreover, in the model equation the "*n*" (diffusion coefficient) gives information about the drug release mechanism. For both kinetics the release exponent was found to be 0.16 and 0.22 for pH 7.4 and 5.0, respectively. A *n* value lower than 0.5 means that the release of Metvan from NLCs was mainly governed by diffusion of the drug out of the carrier (Fickian diffusion) [20,22,23].

Citotoxicity assay

Cell viability studies, determined by the MTT assay [24], were carried out for NLCs (control), NLCs-Mv and free Metvan with MG-63 (human osteosarcoma).

Results showed that not loaded NLCs reduced cell viability to 80.1 ± 9.2% and 81.5 ± 5.6% for 25 µM and 50 µM equivalent to NLCs amount of those used for NLCs-Mv), respectively (**Figure 4**). This basal effect was considered mild and similar to what has been reported for this kind of nanocarriers [19]. Free Metvan incubation generated a significant reduction on cell viability ($p < 0.05$). While 72.0 ± 4.0% of cell viability was found for 25 µM, 65.3 ± 6.8% was exhibited for 50 µM. However, no significant differences were observed between both Metvan concentrations ($p > 0.05$). On the other hand, NLCs-Mv showed the strongest cytotoxic effects at both tested concentration levels. Cell viability reduction to 53.5 ± 4.8% (25µM) and 28.5 ± 1.4% (50µM) were achieved showing significant differences between them and, also, in comparison with free Metvan group ($p < 0.05$) (**Figure 4**). Besides, NLCs-Mv exhibited a cytotoxic effect dependence correlated within drug concentration. This considerable enhancement on cellular effects can be related to the stability of the metal complex inside the nanoparticle core, in addition to the sustained release of the drug from the nanocarrier once inside the cell. It becomes relevant to mention that the experiment design allowed to observe only the effect of those Metvan molecules and NLCs-Mv that could enter to the cell during the first six hours period of exposition. This fact should not be considered trivial since the experiment compare directly the intracellular effects of the nanoformulation against the free drug.

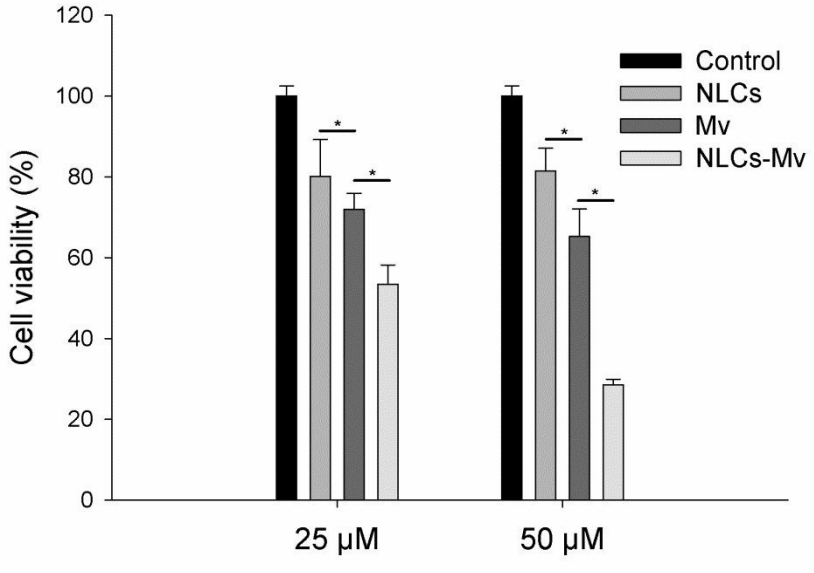

View Article Online
DOI: 10.1039/C9NJ01634A

Figure 4. Cytotoxicity assays against MG-63 cells. Free Metvan (Mv), unloaded NLCs and NLCs loaded with 25 and 50 μM Metvan (NLCs-Mv). Data are expressed as the means ± SD (n = 3). Significant differences at $p < 0.05$ (*) level vs. control untreated cells (ANOVA test).

Cellular uptake of NLCs

In order to evaluate cellular uptake, the fluorescent probe DiOC18 was selected for labeling the NLCs. The fluorescent probe was 100% encapsulated, and no release was observed under our experimental conditions (data not shown). Cells were incubated with labeled NLCs for 1, 3 and 6 h using three different NLCs concentrations. Next, fluorescent signal was analyzed by flow cytometry (**Figure 5A**). First, the results showed that MG-63 cells were capable to incorporate NLCs. Nanoparticles uptake increased over time between 1 and 6 h of exposition. Besides, it was observed that cellular uptake depends on the amount of NLCs in contact with the cells. Since no decrease on uptake rates was observed, it was suggested that the cells were not exposed to saturation levels of nanoparticles during the exposition times.

In order to confirm the observations obtained by flow cytometry, fluorescence microscopy studies were performed. NLCs labeled with DiOC18 probe were incubated with cells for 1 and 6 h. Later, endocytic cellular structures were stained with Lysotracker Red and cell nuclei with DAPI. Microscopy images were not able to show any fluorescent signal corresponding to DiOC18 after the first hour. However, after 6 h of exposition it was possible to observe NLCs presence (**Figure 5B**). Besides, colocalization between NLCs signal and stained lysosomes (white arrows) was detected suggesting the intracellular target organelle of the NLCs once incorporated.

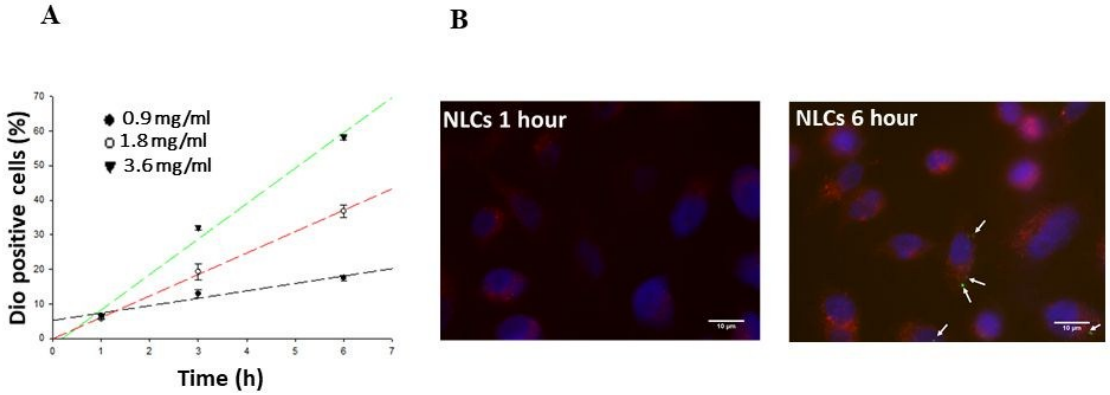

Figure 5. Cellular uptake of NLCs loading DiOC18 fluorescent probe. A) Cells were incubated for different times with 0.9, 1.8 and 3.6 mg/ml of NLCs (equivalent amount for

25, 50 and 100 µM NLCs-Mv). Then, the cells were recorded by flow cytometry. Data is presented as a mean ± standard error (n= 3) with a significance of $p< 0.05$ from empty NLCs control (*) or free Metvan (#). B) Fluorescence microscopy of green-labeled nanoparticles cellular uptake at times 1 h and 6 h. Nuclei were stained with 4,6-diamino-2-phenylindole DAPI (blue) and endocytic structures with Lysotracker™ Red (red). Representative images of triplicate experiments are shown.

Apoptosis

Apoptosis is a physiological process of cell death enhanced in the presence of injurious drugs, characterized by morphological and biochemical changes. One of the first modifications occurring is the externalization of phosphatidylserine at the outer plasma membrane leaflet. Annexin V–FITC is a fluorescent dye with high affinity for phosphatidylserine allowing its determination by fluorescence assays. [25]

To explore whether free Metvan and NLCs-Mv also induced apoptosis, MG-63 cells were stained with Annexin V-fluorescein isothiocyanate and propidium iodide after incubation with NLCs, free Metvan and NLCs-Mv. The results showed that Metvan generated a cytotoxic effect through induction of apoptosis in a concentration-dependent manner observing an increment on late apoptotic cells (V+/PI+) from 6.2% to 27.9% for 25µM and 50 µM, respectively (**Figure 6 A & SM1**). In comparison, NLCs-Mv showed a stronger increment on the number of apoptotic cells specially in late apoptosis (**Figure 6B**). Considering the top quadrants from the dotplots on **Figure SM1**, it can be analyzed that Metvan generated 9.5% and 35.2% of dead cells for 25 µM and 50 µM, respectively. When cells were exposed to NLCs-Mv the numbers raised to 69.7% and 90.0% for 25 µM and 50 µM, respectively. These results are in agreement and confirmed the observations described on cell viability tests. Besides, apoptosis induction by NLCs-Mv exhibited a strong concentration dependence (**Figure 6**). On the other hand, unloaded NLCs showed very low levels of apoptotic cells. The remarkable apoptosis potential of NLCs-Mv was attributed to higher accumulation of the drug in the cancer cells and, specially, because of the suggested protection effect that Metvan molecules might be experiencing. As a comparison, encapsulation of other metallodrugs with poor stability was also reported. For example, Ruthenium complexes have displayed excellent anticancer properties, but their effectiveness was questioned owing to their poor stability in physiological conditions and short half-life time in aqueous media. The generation of

lipid nano-aggregates and liposomal formulations of ruthenium lead to an increase of its stability and consequent better anticancer activity [26,27]. In addition, gold(I) and gold(III) complexes also showed interesting cytotoxic activity against cancer cells [28,29]. However, their potentiality has been undermined by the slight stability and *in vivo* toxicity [30]. To overcome these drawbacks, nanoencapsulation of these complexes has been studied. Gold complexes were encapsulated into polymeric nanoparticles achieving an increase on stability and IC_{50} values on several cancer cell lines much lower than those of cisplatin [31,32]. Other nanoformulations were also described as an option to overcome problems subjected to other metallodrugs such as platinum, iron and titanium based complexes [14]. Our present results indicated for the first time that encapsulating a Vanadium compound into nanocarriers could greatly improve anticancer effects. Moreover, NLCs can serve as an excellent carrier for optimizing Metvan anticancer effects.

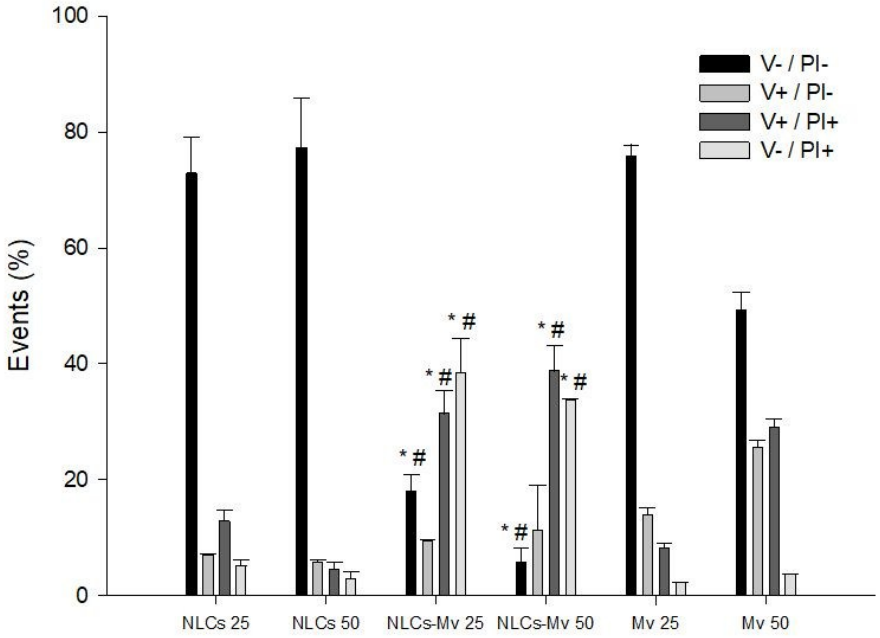

Figure 6. Apoptotic effects of free Metvan (Mv), NLCs and NLCs-Mv at 25 µM and 50 µM after incubation with MG-63 cells. Representation showing the number of events at the different stages: viable cells (V-/PI-), early apoptosis (V+/PI-), late apoptosis (V+/PI+) and dead or necrotic cells (V-/PI+).

Conclusion

NLCs formulation was optimized by QbD approach for the forward encapsulation of Metvan. Optimization process concluded that the desirable formulation consisted in 505.0 mg of lipid, 4.0% p/v of surfactant in aqueous medium and 83% of sonication amplitude. After validation studies, the synthesis process showed high reproducibility. Nanoencapsulation of an active ingredient can provide several advantages such as protection, better administration and sustained release. Therefore, a reduction on adverse effects and an increase in cellular effects might be achieved. In this sense, NLCs exhibited high encapsulation efficiency and sustained release of Metvan after 48 hours. Drug release showed to be pH dependent and mainly governed by the diffusion of the drug out of the carrier (Fickian diffusion). Additionally, Metvan loaded NLCs exhibited a higher *in vitro* effect against osteosarcoma cancer cell line than free Metvan. NLCs-Mv showed the strongest cytotoxic effects dependent of drug loading, in comparison with free Metvan treatment. We hypothesized that the enhancement on cellular effects is related to the protection of the metal complex inside the nanoparticle core while the drug is being released in a sustained manner. Furthermore, apoptosis studies confirmed the previous observations showing that once Metvan was vehiculized in NLCs, its cytotoxic effects were enhanced. These results suggested that Metvan delivery by lipid nanocarriers optimize the biological effects of this vanadium compound. Our approach opens a debate about whether the drawbacks of Metvan for cancer treatment could be addressed by use of novel drug delivery strategies.

Experimental

Materials

The solid lipids myristyl myristate (tetradecyl tetradecanoate), cetyl esters (Crodamol™ SS), cetyl palmitate (hexadecyl hexadecanoate) and the liquid lipid (oil) Crodamol™ GTCC-LQ were kindly donated by Croda (Argentina). Stearic acid (octadecanoic acid), Pluronic®F68, Pluronic®F127, Tween 20, Tween 85 and 3,3-dioctadecyloxacarbocyanine perchlorate (DiOC18) were provided by Sigma–Aldrich (Buenos Aires, Argentina). Other reagents were of analytical grade from available commercial sources and used as received from Merck (Darmstadt, Germany).

Dulbecco's Modified Eagles Medium (DMEM) and TrypLE™ were from Gibco (Gaithersburg, MD, USA), and fetal bovine serum (FBS) from Internegocios SA (Argentina). Annexin V, Fluorescein isothiocyanate (FITC)/PI and tetrazolium salt MTT

(3-(4,5-dimethylthiazol-2-yl)-2,5-diphenyl-tetrazolium-bromide) from Invitrogen Corporation (Buenos Aires, Argentina).

Synthesis of the Metvan

The complex was obtained, as previously described [10] by slow addition of an aqueous solution containing 0.25 mmol of $VOSO_4 \cdot 5H_2O$ to an ethanolic solution containing 0.5 mmol of 4,7-dimethyl-1,10-phenathroline. The reaction mixture was stirred at room temperature for 48 h. The brown solid product was obtained removing the solvent and was washed with chloroform and ether and finally dried under a vacuum. Its purity was confirmed by elemental chemical analysis (Calcd. For $[VO(SO_4)\ (Me2phen)_2] \cdot 3H_2O$; C, 53.08; H, 4.77; N, 8.84; S, 5.06; found C, 53.00; H, 4.83; N, 8.82; S, 5.02%).

Nanostructured lipid carrier (NLC) preparation

NLCs containing Metvan were prepared by sonication method [33]. Quantities of each NLC components were modulated during the optimization of the formulation. Briefly, different amounts of solid lipids (100-568.18 mg) were melted under water bath at 60°C and, in the case of NLCs-Mv, were mixed with 5 mg of Metvan (dissolved in 100 µL of DMSO). Liquid lipid (oil) (0.06%, v/v) was incorporated. After 10 min, a hot aqueous solution (20 mL) containing 600 mg (6%, w/v) of Pluronic® F127 was added to the lipid phase. Immediately, the mixture was sonicated for different time periods with different amplitudes using an ultrasonic processor (130 W, Cole-Parmer, USA) equipped with 6 mm titanium tip. Then, the dispersion was cooled at room temperature and stored at 5°C. Formulations used for the optimization process lack of drug loading due to the small amount of the active principle available for this work. Once the formulation was optimized, Metvan was incorporated to the synthesis process.

Metvan detection was performed by UV–vis spectroscopy. An intense and stable peak was detected at 270 nm wavelength. Metvan calibration curves were performed in the range from 2.5 to 50.0 µM in phosphate buffer (pH 7.4, 10 mM), acetate buffer (pH 5.0, 10 mM) and in acetonitrile (ACN).

Particle size, zeta potential and poly-dispersity index (PDI)

The average diameter and size distribution of lipid nanoparticles were measured by photon correlation spectroscopy (PCS) (Nano ZS Zetasizer, Malvern Instruments Corp, UK) at 25 °C in polystyrene cuvettes with a thickness of 10 mm. The zeta potential was

determined by laser Doppler anemometry also using the Nano ZS Zetasizer. The zeta potential measurements were performed in capillary cells, for the NPs dispersed in deionized water obtained from Milli-Q system (Millipore, MA, USA). Also, the PDI value was determined. All the measurements were carried out in triplicate and the average values ±S.D. were calculated.

Transmission electron microscopy (TEM)

The nanoparticle dispersion was 10-times diluted with ultrapure water and a drop of the dispersion was spread onto a collodion-coated Cu grid (400-mesh). Liquid excess was drained with paper filter (Whatman #1) and for contrast enhancement a drop of phosphotungstic acid as added to the NLCs dispersion. Finally, TEM analysis was performed using Jeol-1200 EX II-TEM microscope (Jeol, MA, USA).

Screening of solid lipids for NLC preparation

Before proceeding to the optimization of NLCs formulation by QbD, four different solid lipids and four surfactants were tested using a two-way factorial design. Different formulations were synthesized from the combination between the lipids myristyl myristate (MM), cetyl esters (SS), cetyl palmitate (CP) and stearic acid (SA), and the surfactants Pluronic® F68, Pluronic® F127, Tween 20 and Tween 85. All the syntheses were performed setting the amount of lipid to 400 mg (2%, w/v), oil to 100 µl (0.06%, v/v) and surfactant to 600 mg (6%, w/v). Besides, the sonication process was set to 30 minutes and 70% of amplitude at 70ºC. As a result, sixteen formulations were obtained and analyzed by DLS for apparent diameter, Z-potential and PDI. The lipid and surfactant that generated the smallest diameter and PDI values, and the Z-potential between 0 and +20 mV was chosen to continue with the optimization process.

Optimization of the formulations through fractional factorial design and CCD/response surface methodology

A fractional factorial design was used to simultaneously study the effect of multiple factors over the selected responses or dependent variables: mean particle size (d), polydispersity index (PDI) and zeta potential (Z pot). A resolution V randomized fractional factorial design (2^{k-1}) was employed in order to reduce the number of runs. A total of k=5 factors at two levels were studied: amount of lipid (X_1), surfactant percentage

View Article Online
DOI: 10.1039/C9NJ01634A

in aqueous medium (X_2), amount of oil (X_3), sonication time (X_4) and sonication amplitude (X_5). The factors levels were selected based on previous experience [34,35] (**Table 1**). Analysis of variance (ANOVA) was applied to determine the factors with statistically significant influence on the responses. Statistical calculations were made with the R package "FrF2" and RStudio software [36–38].

A CCD and the associated RS were used for the final optimization of the formulation. To do so, three (out of five) factors were selected for further evaluation: amount of lipid, surfactant percentage in aqueous medium and sonication amplitude, based on the results of the previous fractional factorial design. Alpha value was set at 1.682 to generate a spherical rotatable design (the α value is defined as the distance of the axial runs from the center of the design and equals the fourth root of the number of factorial runs ($(2^3)^{1/4} = 1.682$)[39]. Each factor was evaluated in the CCD at 5 different levels: -α, -1, 0, 1 and α, with 5 replications at the center point (**Table 2**). "Desirability" and "rsm" R packages were used for calculations [17,40].

Measurement of encapsulation efficiency and loading capacity

Metvan encapsulation or entrapment efficiency (EE%) and loading capacity (LC%) of NLCs were determined by measuring the concentration of free drug in the aqueous phase of the dispersion, after filtration-centrifugation. Briefly, 500 µl of NLCs were transferred to an ultrafiltration centrifugal device (MWCO 10,000, Microcon, Millipore, MA, USA) and centrifuged at 5000 ×g at 5ºC for 10 min. The non-encapsulated Metvan was measured by UV–vis spectroscopy (λ_{max} = 270 nm). It has been verified that the presence of lipids and other components did not interfere with the UV spectrophotometric assay of the drug. EE% and LC% of Metvan in the NLC were calculated according to the following equations:

$$EE\% = \frac{W_{initial\ drug} - W_{free\ drug}}{W_{initial\ drug}} \times 100 \quad (1)$$

$$LC\ \% = \frac{W_{initial\ drug} - W_{free\ drug}}{W_{lipid}} \times 100 \quad (2)$$

Where $W_{free\ drug}$ is the amount of free drug detected in the filtrate, W_{lipid} is the amount of the total lipid used and $W_{initial\ drug}$ corresponds to the total amount of drug in the formulation. The determination of the total amount of the drug present in the formulation was determined by the direct method after NLCs synthesis. Basically, 500 µl of NLCs where mixed with 1000 µl of acetonitrile. Next, the solution was vortexed and centrifuged

at 5000 ×g at 5ºC for 10 min. The total amount of Metvan was determined from the supernatant using the corresponding calibration curve.

The determinations of EE% and LC% are expressed as the mean of three separate experiments.

Drug release assays

Experiments were performed using dialysis membranes (MWCO 10 kDa.). The membranes were soaked with distilled water for 12 h and filled with 2.5 mL of each formulation of NLCs, followed by immersion in 30 mL of 10mM acetate buffer (pH= 5.0) or 10 mM phosphate buffer (pH= 7.4) at 37°C, with continuous shaking at 200 rpm. At different times, samples of 10 mL were withdrawn, and drug concentration was measured spectrophotometrically.

To examine the drug release kinetics, the release data were fitted to models representing First Order (3), Higuchi (4) and Korsmeyer–Peppas (5) [22]:

$$\log M_t = \log M_0 + \frac{k_1}{2.303} t \quad (3)$$

$$M_t = M_0 + k_H t^{1/2} \quad (4)$$

$$M_t = k_{KP} t^n \quad (5)$$

where M_0 is the initial amount of Metvan, M_t is the cumulative amount of drug release at time "t", k_1 is the first-order release constant, k_H is the Higuchi constant, k_{KP} is the Korsmeyer–Peppas constant and n is an exponent value which gives information about the release mechanism. The best fitting model with the experimental data was selected based on the highest correlation coefficient (r^2) values. SigmaPlot 11.0 software was used to analyze the data and perform the modelling tests.

Cell line and growth conditions

Human osteosarcoma cell line (MG-63) was grown in Dulbecco's modified Eagle's medium (DMEM) containing 10% fetal bovine serum (FBS), 100 IU/mL penicillin and 100 µg/mL streptomycin at 37°C in 5% CO_2 atmosphere. MG-63 cell line was grown in a 75 cm^2 flask until they reach 70–80% of confluence. Then, the cells were subcultured using TrypLE ™. For experiments, cells were grown in multi-well plates. Dulbecco's modified Eagle's medium (DMEM) and TrypLE ™ and fetal bovine serum (FBS). After

View Article Online
DOI: 10.1039/C9NJ01634A

24 h the monolayers were washed with DMEM and were incubated under different conditions according to the experiments.

Cytotoxicity study: 3-(4,5-Dimethylthiazol-2-yl)-2,5-diphenyltetrazolium bromide assay

The 3-(4,5-dimethylthiazol-2-yl)-2,5-diphenyltetrazolium bromide (MTT) assay was performed according to [24]. Briefly, cells were seeded in a 96-well dish, allowed to attach for 24 h, and treated with different concentrations of ruthenium complexes at 37º C for 24 h. Afterward, the medium was changed and the cells were incubated with 0.5 mg/mL MTT under normal culture conditions for 3 h. Cell viability was marked by the conversion of the tetrazolium salt MTT to a colored formazan by mitochondrial dehydrogenases. Color development was measured spectrophotometrically with a microplate reader (multiplate reader multiskan FC, thermo scientific) at 570 nm after cell lysis in DMSO (100 µL per well). Cell viability was plotted as the percentage of the control value.

NLCs cellular internalization studies

The cellular uptake of NLCs was studied by incorporation of the green fluorescent dye DiOC18 (484/501 nm) to the nanoparticles. Briefly, 1.0 mg of the lipophilic tracer was mixed with the melted lipid phase (at 60ºC) until total dissolution and protected from light. The nanoparticles were prepared as previously described. As a result, the dye was 100% encapsulated into the NLCs. The cellular uptake of fluorescent-labeled NLC was evaluated by flow cytometry and fluorescence microscopy.

For flow cytometry studies, cells were seed for 24 h in standard 24-well plates at 8×10^4 cells per well. Three different concentrations of NLCs were added to the cells (0.9, 1.8 and 3.6 mg/ml) and incubated for different periods of time (1, 3 and 6 h). At the end of each period cells were washed twice with PBS. Then, cells were treated with 300 µl of trypsin and then 1.0 mL of medium was added to each well. Next, samples were collected from each well to cytometry tubes and centrifuged at 2500×g for 5 min. Supernatant was discarded and cells were re-suspended in 350 µL of FACs buffer. Fluorescence intensity was monitored using a FACSCalibur (Becton–Dickinson, Franklin Lakes, NJ, USA) and analyzed using FlowJo 7.6 software.

Fluorescence microscopy was performed using a Leica DM 2500 microscope (Wetzlar, Germany). MG- 63 cells were plated in collagen-coated cover glasses on 24 well-plates

at density of 100,000 cells/mL incubated at 37°C for 24 h. Thereafter, cells were exposed to NLCs at a concentration of 7.2 mg/ml. After 6 h incubation, medium was discarded, and cells were washed three times with PBS. Next, Lysotracker Red (15 μM, Invitrogen, MA, USA) was added to each well and incubated at 37°C for 20 m. After then, cells were washed with PBS, fixed with paraformaldehyde 4.0% at room temperature for 30 m and mounted with ProLong® Gold Antifade Reagent with 4′,6- diamidino-2-phenylindole dihydrochloride (DAPI, 350/470 nm) for nuclear staining (Life Technologies, Carlsbad, CA, USA).

Apoptosis

Cells in early and late stages of apoptosis were detected with Annexin V-FITC and propidium iodide (PI) staining. Annexin V, fluorescein isothiocyanate (FITC), and propidium iodide (PI) were from Invitrogen (Buenos Aires, Argentina). Cells were treated with the three complexes and incubated for 24 h prior to analysis. For the staining, cells were washed with PBS and were diluted with 1X binding buffer. To 100 μL of cell suspension, 2.5 μL of Annexin V-FITC and 2 μL PI (250 μg/mL) were added and incubated for 15 min at room temperature prior to analysis. Cells were analyzed using flow cytometer (BD FACS Calibur™) and FlowJo 7.6 software. For each analysis 10,000 counts, gated on FSC vs SSC dot plot, were recorded. Four subpopulations were defined in the dot plot: the undamaged vital (Annexin V−/PI−), the vital mechanically damaged (Annexin V/PI+), the apoptotic (Annexin V+/PI−), and the secondary necrotic (Annexin V+/PI+) subpopulations.

Acknowledgments This work was partly supported by UNLP (11X/690), CONICET (PIP 0034), and ANPCyT (PICT 2014-2223, 2016-1574, 2016-4597) from Argentina and. GRC, MER, EJB, MAF, IEL and RMTS are members of the Carrera del Investigador, CONICET, Argentina. MCR, MLC, SSM have a fellowship from ANPCyT, Argentina.

References

1 M. Frezza, S. Hindo, D. Chen, A. Davenport, S. Schmitt, D. Tomco and Q. P. Dou, *Curr. Pharm. Des.*, 2010, **16**, 1813–25.

2 I. Leon, J. Cadavid-Vargas, A. Di Virgilio and S. Etcheverry, *Curr. Med. Chem.*, 2017, **24**, 112–148.

3 M. Sutradhar, Rajeshwari, T. Roy Barman, A. R. Fernandes, F. Paradinha, C. Roma-Rodrigues, M. F. C. Guedes da Silva and A. J. L. Pombeiro, *J. Inorg. Biochem.*, 2017, **175**, 267–275.

4 I. E. León, N. Butenko, a. L. Di Virgilio, C. I. Muglia, E. J. Baran, I. Cavaco and S. B. Etcheverry, *J. Inorg. Biochem.*, 2014, **134**, 106–117.

5 I. E. León, J. F. Cadavid-Vargas, I. Tiscornia, V. Porro, S. Castelli, P. Katkar, A. Desideri, M. Bollati-Fogolin and S. B. Etcheverry, *J. Biol. Inorg. Chem.*, 2015, **20**, 1175–91.

6 J. C. Pessoa, S. Etcheverry and D. Gambino, *Coord. Chem. Rev.*, 2015, **301**–**302**, 24–48.

7 M. Sutradhar, A. R. Fernandes, J. Silva, K. T. Mahmudov, M. F. C. Guedes da Silva and A. J. L. Pombeiro, *J. Inorg. Biochem.*, 2016, **155**, 17–25.

8 O. J. D'Cruz and F. M. Uckun, *Expert Opin. Investig. Drugs*, 2002, **11**, 1829–1836.

9 R. K. Narla, Y. Dong, D. Klis and F. M. Uckun, *Clin. Cancer Res.*, 2001, **7**, 1094–101.

10 Y. Dong, R. K. Narla, E. Sudbeck and F. M. Uckun, *J. Inorg. Biochem.*, 2000, **78**, 321–30.

11 D. Sanna, V. Ugone, G. Micera, P. Buglyó, L. Bíró and E. Garribba, *Dalt. Trans.*, 2017, **46**, 8950–8967.

12 M. Le, O. Rathje, A. Levina and P. A. Lay, *J. Biol. Inorg. Chem.*, 2017, **22**, 663–672.

13 A. Levina, D. C. Crans and P. A. Lay, *Coord. Chem. Rev.*, 2017, **352**, 473–498.

14 W. A. Wani, S. Prashar, S. Shreaz and S. Gómez-Ruiz, *Coord. Chem. Rev.*, 2016, **312**, 67–98.

15 H. Raina, S. Kaur and A. B. Jindal, *J. Drug Deliv. Sci. Technol.*, 2017, **39**, 180–191.

16 E. V Batrakova and A. V Kabanov, *J. Control. Release*, 2008, **130**, 98–106.

17 M. Kuhn, 2016.

18 N. Oh and J. H. Park, *Int. J. Nanomedicine*, 2014, **9**, 51–63.

19 B. Rodenak-kladniew, G. A. Islan, M. G. De Bravo, N. Durán and G. R. Castro, *Colloids Surfaces B Biointerfaces*, 2017, **154**, 123–132.

20 H. Vaghasiya, A. Kumar and K. Sawant, *Eur. J. Pharm. Sci.*, 2013, **49**, 311–322.

21 S. Jose, J. F. Fangueiro, J. Smitha, T. A. Cinu, A. J. Chacko, K. Premaletha and E. B. Souto, *Eur. J. Med. Chem.*, 2013, **60**, 249–253.

22 D. P. Gaspar, V. Faria, L. M. Goncalves, P. Taboada, C. Remuñan-Lopez and A. J. Almeida, *Int. J. Pharm.*, 2016, **497**, 199–209.

23 M. S. Lobo and P. Costa, *Eur. J. Pharm. Sci.*, 2001, **13**, 123–133.

24 T. Mosmann, *J. Immunol. Methods*, 1983, **65**, 55–63.

25 M. Hassan, H. Watari, A. AbuAlmaaty, Y. Ohba and N. Sakuragi, *Biomed Res. Int.*, 2014, **2014**, 1–23.

26 L. Simeone, G. Mangiapia, G. Vitiello, C. Irace, A. Colonna, O. Ortona, D. Montesarchio and L. Paduano, *Bioconjug. Chem.*, 2012, **23**, 758–770.

27 M. Vaccaro, R. Del Litto, G. Mangiapia, A. M. Carnerup, G. D'Errico, F. Ruffo and L. Paduano, *Chem. Commun.*, 2009, 1404–1406.

28 P. J. Barnard and S. J. Berners-Price, *Coord. Chem. Rev.*, 2007, **251**, 1889–1902.

29 A. Bindoli, M. P. Rigobello, G. Scutari, C. Gabbiani, A. Casini and L. Messori, *Coord. Chem. Rev.*, 2009, **253**, 1692–1707.

30 P. C. A. Bruijnincx and P. J. Sadler, *Curr. Opin. Chem. Biol.*, 2008, **12**, 197–206.

31 S. Pearson, W. Scarano and M. H. Stenzel, *Chem. Commun.*, 2012, **48**, 4695–4697.

32 M. Ahmed, S. Mamba, X. H. Yang, J. Darkwa, P. Kumar and R. Narain, *Bioconjug. Chem.*, 2013, **24**, 979–986.

33 M. L. Cacicedo, G. A. Islan, I. E. León, V. A. Álvarez, I. Chourpa and E. Allard-vannier, *Colloids Surfaces B Biointerfaces*, 2018, **170**, 596–608.

34 G. A. Islan, P. C. Tornello, G. A. Abraham, N. Duran and G. R. Castro, *Colloids Surf. B Biointerfaces*, 2016, **143**, 168–176.

35 S. Scioli Montoto, M. L. Sbaraglini, A. Talevi, M. Couyoupetrou, M. Di Ianni, G. O. Pesce, V. A. Alvarez, L. E. Bruno-Blanch, G. R. Castro, M. E. Ruiz and G. A. Islan, *Colloids Surfaces B Biointerfaces*, 2018, **167**, 73–81.

36 U. Grömping, *J. Stat. Softw.*, 2014, **56**, 1–56.

37 RStudio Team, 2018.

38 R Core Team, R. R Development Core Team and R Core Team, R: A Language and Environment for Statistical Computing.

39 R. H. Myers, D. C. Montgomery and C. M. Anderson-Cook, *Response surface methodology. Process and product optimization using designed experiments*, 2009.

40 R. V. Lenth, *J. Stat. Softw.*, 2009, **32**, 1–17.

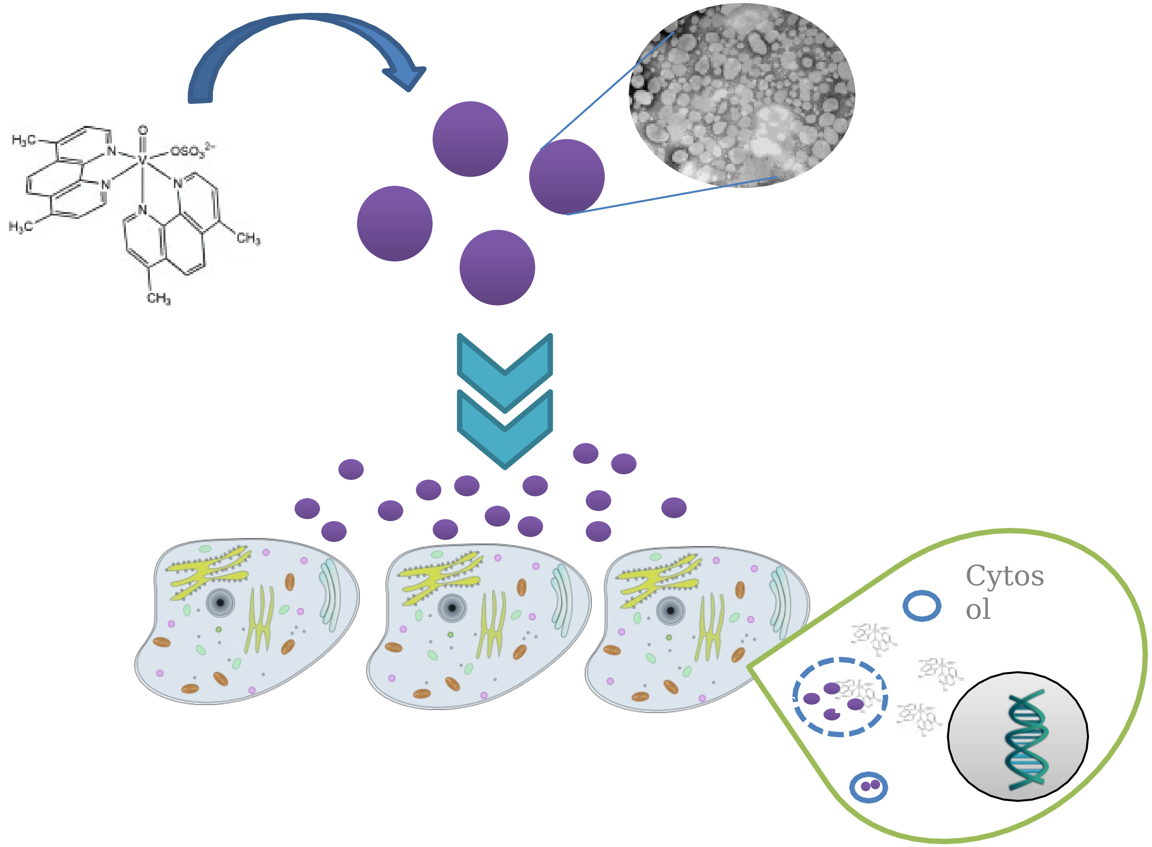

New Metvan-NLCs compound was developed to improving its biopharmaceutical profile and antitumor efficacy.